



1 **An arid early Holocene revealed by palynological evidence for the north-east**  
2 **Tibetan Plateau**

3 Nannan Wang<sup>1,2</sup>, Lina Liu<sup>1,2</sup>, Xiaohuan Hou<sup>1</sup>, Yanrong Zhang<sup>1</sup>, Haicheng Wei<sup>3</sup>, Xianyong Cao<sup>1\*</sup>

4 <sup>1</sup> *Alpine Paleocology and Human Adaptation Group (ALPHA), State Key Laboratory of Tibetan*  
5 *Plateau Earth System, Resources and Environment (TPESRE), Institute of Tibetan Plateau*  
6 *Research, Chinese Academy of Sciences, Beijing 100101, China*

7 <sup>2</sup> *University of the Chinese Academy of Sciences, Beijing 100049, China*

8 <sup>3</sup> *Key Laboratory of Comprehensive and Highly Efficient Utilization of Salt Lake Resources,*  
9 *Qinghai Institute of Salt Lakes, Chinese Academy of Sciences, Xining 810008, China*

10 *Correspondence to:* Xianyong Cao (xcao@itpcas.ac.cn)

11

12 **Abstract.** Situated in the triangle of the East Asian monsoon, the Indian monsoon,  
13 and the westerlies, the Holocene patterns of climate and vegetation changes on the  
14 north-east Tibetan Plateau are still unclear or even contradictory. By investigating the  
15 distribution of modern pollen taxa on the east Tibetan Plateau, we infer the past  
16 vegetation and climate since the last 14.2 ka BP (thousand years before present) from  
17 a fossil pollen record extracted from Gahai Lake (102.3133°E, 34.2398°N; 3444 m  
18 a.s.l.) together with multiple proxies (grain-size, contents of total organic carbon and  
19 total nitrogen) on the north-east Tibetan Plateau. Results indicate that the Gahai Basin  
20 was covered by arid alpine steppe or even desert between 14.2 and 7.4 ka BP with a  
21 mild and dry climate, and high percentages of arboreous pollen are thought to be  
22 long-distance wind transported grains. Montane forest (dominated by *Abies*, *Picea*,  
23 and *Pinus*) migrated into the Gahai Basin between 7.4 and 3.8 ka BP driven by wet  
24 and warm climatic conditions (the climate optimum within the Holocene) but reverted  
25 to alpine steppe between 3.8 and 2.3 ka BP, indicating a drying climate trend. After  
26 2.3 ka BP, vegetation shifted to alpine meadow represented by increasing abundances  
27 of Cyperaceae, which may reflect a cooling climate. The strange pollen spectra with  
28 high abundances of Cyperaceae and total pollen concentrations after ca. 0.24 ka BP



29 (1710 CE) could be an indication of disturbance by human activities to some extent,  
30 but needs more direct evidence to be confirmed. Our study confirms the occurrence of  
31 a climate optimum in the mid-Holocene on the north-east Tibetan Plateau, which is  
32 consistent with climate records from the fringe areas of the East Asian summer  
33 monsoon, and provides new insight into the evolution of the Asian monsoon system.

34 **Keywords:** Gahai Lake; pollen; climate reconstruction; vegetation evolution; last  
35 deglacial

## 36 **1 Introduction**

37 Vegetation, as an essential component in the terrestrial ecosystem, responds to and  
38 represents environmental and climatic changes well. Investigating the patterns and  
39 mechanisms of past vegetation changes can provide a reliable analogue for predicting  
40 future climate and vegetation changes (Mykleby et al., 2017; Zhao et al., 2017). Since  
41 the sharp climate warming during the last deglacial (after ca. 15 ka BP in the Northern  
42 Hemisphere; Wang et al., 2001; Andersen et al., 2004; Dykoski et al., 2005; Xu et al.,  
43 2013), the response of vegetation to climate warming could be a valuable palaeo-  
44 analogue for understanding current vegetation changes under global warming and for  
45 predicting future vegetation trends (Birks, 2019).

46 The north-east Tibetan Plateau lies in the transition between the East Asian summer  
47 monsoon, the Indian summer monsoon, and the westerlies; it is sensitive to climate  
48 change and is an ideal region to study past vegetation and climate variation (Bryson,  
49 1986; An et al., 2012; Chen et al., 2016). Nevertheless, the climate records from  
50 different lacustrine sediments on the north-east Tibetan Plateau show a lack of  
51 consistency, for example, regarding the climatic conditions during the early Holocene.  
52 Some records reveal that the climate was relatively dry on the north-east Tibetan  
53 Plateau and controlled by the East Asian monsoon during the early Holocene (Shen et  
54 al., 2005; Herzschuh et al., 2006; Cheng et al., 2013), while other records such as  
55 those from Hala Lake and Genggahai Lake show that there was maximum water  
56 depth and hence climatic optimum in the early Holocene (Qiang et al., 2013; Yan and



57 Wünnemann, 2014; Wang et al., 2021). Therefore, more studies are needed to clarify  
58 the early Holocene climatic conditions, which are necessary to resolve the  
59 environmental evolution of the north-east Tibetan Plateau.

60 Pollen plays an important role in reconstructing the past vegetation and climate owing  
61 to its preservation in various sediment types (Chevalier et al., 2020). However, pollen-  
62 based vegetation and climate reconstructions on the Tibetan Plateau are also  
63 confronted with challenges, for instance, the current quantitative reconstructions of  
64 vegetation and climate are based on pollen percentages, which can be biased when  
65 there is much exogenous arboreal pollen, especially in strata with extremely low  
66 pollen concentrations because the exogenous arboreal pollen will enlarge its  
67 proportion in the pollen spectra (Herzschuh, 2007; Ma et al., 2017; 2019). Exogenous  
68 arboreal pollen can be recognised in areas far away from forested regions, mainly  
69 because no trees grow around the lake or its adjacent areas nowadays, such as  
70 Luanhaizi Lake (Herzschuh et al., 2010), Donggi Cona Lake (Wang et al., 2014),  
71 Hala Lake (Hu et al., 2016), and Kuhai Lake (Wischnewski et al., 2011). Arboreal  
72 pollen can then be excluded in subsequent analysis to ensure the correct interpretation  
73 of vegetation and environment. However, it is somewhat difficult to recognise the  
74 contribution of exogenous pollen from areas near the forest on the eastern part of the  
75 Tibetan Plateau, which could seriously impact the results of pollen reconstruction,  
76 such as from Naleng Lake (Kramer et al., 2010a) and Qinghai Lake (Shen et al.,  
77 2005). Solving this issue of clarifying the influence of exogenous pollen is an  
78 important prerequisite for a better understanding of the early Holocene climate.  
79 Understanding the spatial distribution characteristics of modern pollen and their  
80 relationships may be an effective way to identify such arboreal pollen.

81 In this study, we integrate multi-proxy records (pollen, grain size, total organic carbon  
82 (TOC), total nitrogen (TN)) of Gahai Lake to reconstruct the climate and vegetation  
83 evolution since the last deglacial. We assess the dispersal ability and biotopes of the  
84 main pollen taxa in the pollen record by investigating the distribution of modern  
85 pollen and their relationship with climate. We attempt to recognise exogenous pollen



86 and evaluate its influence on reconstruction results to determine whether the early  
87 Holocene of the north-east Tibetan Plateau was dry or wet.

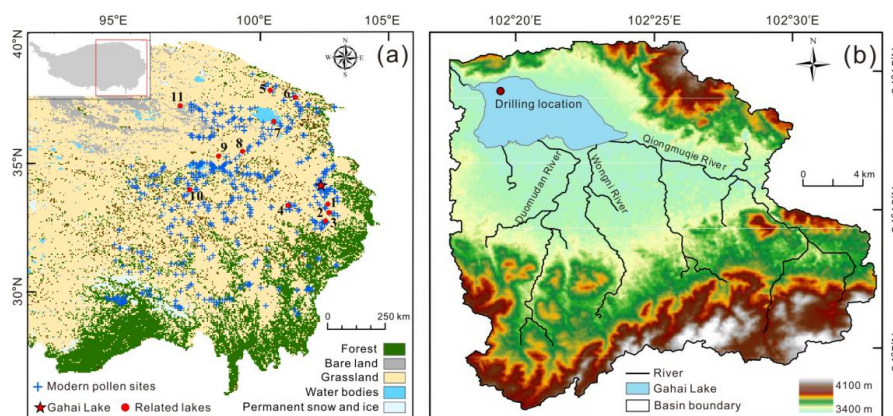
## 88 **2 Study area**

89 Gahai Lake (102.3133°E, 34.2398°N; 3444 m a.s.l.) is situated in the upper reaches of  
90 the Yellow River on the north-east Tibetan Plateau, a transitional zone between the  
91 Tibetan Plateau, the mountainous area of Longnan, and the Loess Plateau (Fig. 1).  
92 Gahai Lake is a typical plateau interior freshwater lake, with a total area of 15 km<sup>2</sup>  
93 and a mean water depth ranging from 2 to 2.5 m. The water supply of the lake is  
94 mainly from precipitation, groundwater recharge, and surface runoff from surrounding  
95 mountains to the south and south-east including Qiongmuequ, Wenniqu, and  
96 Geqionguhe rivers, and there is a single outflow stream at the north-western end of  
97 the basin (Duan et al., 2016; Fig. 1). Gahai Lake belongs to the alpine humid climate  
98 zone, which is influenced by the West Pacific Subtropical High in summer and  
99 controlled by westerlies in winter. Climate characteristics are rain in the warm season,  
100 and large seasonal and diurnal temperature differences (Liang, 2006). Mean annual  
101 temperature of this region is 1.2°C and mean annual precipitation is 782 mm, with  
102 about 80% of precipitation falling in the rainy season (from June to September), and  
103 mean annual evaporation is 1150 mm (Duan et al., 2016).

104 Vegetation cover in Gahai Basin exceeds 90%. There are abundant species in the  
105 grassland community, which is the intersection between various flora, and perennial  
106 herbs predominate. The dominant plant species include *Poa annua*, *Carex*,  
107 *Clintoniaudensis*, *Polygonum*, *Ranunculus japonicus*, *Potentilla fruticosa*, *Neyraudia*  
108 *reynaudiana*, and *Elymus nutans*. Forest is found in the eastern low mountains with a  
109 mosaic distribution of meadow and shrub, dominated by *Abies*, *Picea*, *Betula*, and  
110 Cupressaceae. *Picea* is found in damp areas at the foot of mountains and replaced by  
111 *Betula* as a transitional community after being cut down; *Abies* occurs on shady and  
112 semi-shady slopes between 3200 and 3400 m a.s.l.; Cupressaceae is distributed mostly  
113 on sunny and semi-sunny slopes of more than 35 degrees. This region belongs to a



114 typical stockbreeding district, and the grazing activity focuses on the grassland. In  
115 addition, there is small-scale agricultural along the river valley at low elevations  
116 (Liang et al., 2006; Duan et al., 2016).



117  
118 **Figure 1.** (a) Land-use map of the eastern Tibetan Plateau (Du, 2019). Lakes referred to in the text:  
119 1, ZB08-C1; 2, ZB10-C14; 3, Hongyuan peatland; 4, Ximencuo Lake; 5, Dalianhai Lake; 6,  
120 Luanhaizi Lake; 7, Qinghai Lake; 8, Kuhai Lake; 9, Donggi Cona Lake; 10, Koucha Lake; 11,  
121 Hurleg Lake. (b) Catchment map of Gahai Lake.

### 122 3 Material and methods

#### 123 3.1 Modern pollen data and their climate data

124 Our modern pollen dataset ( $n=731$ ) is derived from the east Tibetan Plateau ranging  
125 from 94.07 to 103.02°E and from 29.13 to 38.48°N, with elevations from 2515 to  
126 5008 m a.s.l.. These modern pollen data are mainly from the modern pollen database  
127 of China and Mongolia (Cao et al., 2014) and recently published pollen data for the  
128 east Tibetan Plateau (Cao et al., 2021; Wang et al., 2022). The pollen sites are  
129 generally evenly distributed across the east Tibetan Plateau, covering subalpine forest,  
130 alpine meadow, alpine steppe, and alpine desert (Fig. 1). Pollen sample types include  
131 topsoil, lake surface-sediments, and moss polsters mainly.

132 We selected four important climate variables including mean annual precipitation  
133 ( $P_{ann}$ ), mean temperature of the warmest month ( $Mt_{wa}$ ), mean temperature of the



134 coldest month ( $Mt_{co}$ ), and mean annual temperature ( $T_{ann}$ ), together with elevation  
135 (Elev) to investigate the relationship between pollen assemblages and environment  
136 following previous studies (Lu et al., 2011; Herzsuh et al., 2011; Cao et al., 2021;  
137 Wang et al., 2022). Modern climatic data were obtained from the Chinese  
138 Meteorological Forcing Dataset (CMFD; gridded near-surface meteorological dataset),  
139 and each sample is assigned to the nearest pixel of the CMFD using the *fields* package  
140 version 13.3 (Nychka et al., 2021) of R (version 4.0.3; R Core Team, 2021). The  
141 detailed processes of obtaining climatic data are presented in the Fig. A1.

### 142 *3.2 Sediment sampling and radiocarbon dating*

143 A 329-cm-long sediment core (named GAH) was obtained using a UWITEC platform  
144 from the deepest part of Gahai Lake (ca. 2 m) in January 2019 (Fig. 1), and then  
145 transported to the Institute of the Tibetan Plateau Research for preservation. GAH was  
146 sub-sampled at 1 cm intervals, and all sub-samples were freeze-dried.

147 The age-depth model for GAH was established by  $^{210}\text{Pb}$ ,  $^{137}\text{Cs}$ , and accelerator mass  
148 spectrometry (AMS) radiocarbon dating. The top 20 cm of the sediment at 1-cm  
149 intervals was measured for  $^{210}\text{Pb}$  and  $^{137}\text{Cs}$  at the School of Geographical Science,  
150 Nantong University. The constant rate of supply (CRS) model was selected to  
151 calculate the dates due to the non-monotonic variation of unsupported  $^{210}\text{Pb}$  activity,  
152 as the results revealed that the  $^{210}\text{Pb}$  dates were inconsistent with the  $^{137}\text{Cs}$  peak of  
153 1963 CE (Appleby, 2001). To solve this problem, the core was divided into two  
154 sections using  $^{210}\text{Pb}_{ex}$  activity variation data using different formulae to calculate the  
155 dates and obtain a good effect. Finally, an age-depth model based on a  $^{210}\text{Pb}$ -CRS  
156 model corrected by  $^{137}\text{Cs}$  peak was generated (Fig. 4a). Twelve bulk organic sediment  
157 samples of 1-cm thickness were sent for AMS  $^{14}\text{C}$  dating by Beta Analytic Inc., USA,  
158 owing to a lack of macrofossils (Table 2). The age-depth model was established using  
159 the Bayesian age–depth modelling in the *rbacon* package (version 2.5.7; Blaauw and  
160 Christen 2011; Blaauw et al., 2021) in R (R Core Team 2021) and the IntCal20  
161 radiocarbon calibration curve (Reimer et al., 2020).



162 *3.3 Laboratory analysis*

163 The pollen samples (0.6–22 g;  $n=111$ ; at 1 to 2 cm intervals) were treated with  
164 hydrofluoric acid sieving-analysis (Fægri and Iversen, 1975). *Lycopodium* spores (ca.  
165 27,560 grains) were added to the samples to calculate the pollen concentration, then  
166 samples were processed with 10% HCl, 10% KOH, and 36% HF, and sieved through  
167 a 7  $\mu\text{m}$  nylon mesh, followed by acetolysis (9:1 mixture of acetic anhydride and  
168 sulphuric acid) treatment. Finally, glycerin was added to preserve the samples. The  
169 pollen taxa were identified and counted with a 400x LEICA DM 2500 optical  
170 microscope, with the aid of modern pollen reference slides collected from the eastern  
171 and central Tibetan Plateau (including 401 common species of alpine meadow; Cao et  
172 al., 2020) and published atlases for pollen and spores (Wang et al., 1995; Tang et al.,  
173 2017). At least 100 terrestrial pollen grains were counted for most samples, except for  
174 10 samples owing to extremely low pollen concentration; and more than 3000  
175 *Lycopodium* spores were counted for each sample above 176 cm. Because of the low  
176 pollen concentrations below the depth 176 cm, only pollen data for the upper part of  
177 the core are presented and discussed.

178 For the grain-size analysis, freeze-dried samples (1 g;  $n=176$ ; above 176 cm) were  
179 treated with 30%  $\text{H}_2\text{O}_2$  to remove organic matter and 10% HCl to remove carbonate,  
180 cleaned with deionized water and kept stable for 24 h, before adding 0.5 N sodium  
181 hexametaphosphate (10 ml) and undergoing ultrasonic cleaning for 10 minutes. A  
182 laser diffraction particle size analyser MASTERSIZER 3000 (Chen et al., 2013) was  
183 used, with each sample being tested 3 times and their average value used in the final  
184 grain-size data.

185 A total of 176 samples were analysed to obtain organic matter change since the last  
186 deglacial, including TN and TOC. Catalysts were added to freeze-dried samples and  
187 reacted quickly. TN was measured with an Elementar element analyser (CNS analyser,  
188 Vario MAX Cube)/Elementar Vario EL III which has a measurement accuracy of  
189 0.001. TOC was measured with a Vario MAX C analyser, and has the same accuracy  
190 as TN. All samples were ground to ensure sufficient reaction before testing. The C/N



191 ratio was calculated by dividing TOC by TN.

### 192 *3.4 Numerical analyses*

193 Ordination analyses were employed to investigate the modern relationship between  
194 pollen taxa and climatic variables for the eastern Tibetan Plateau. Pollen taxa (with  
195  $\geq 10\%$  maximum and  $\geq 30$  occurrences) from the 731 modern pollen assemblages were  
196 used for detrended correspondence analysis (DCA; Hill and Gauch, 1980). The length  
197 of the first axis of the pollen data was 3.29 SD (standard deviation units), indicating  
198 that a linear response model is suitable for the modern pollen dataset (ter Braak and  
199 Verdonschot, 1995). Hence, we performed redundancy analysis (RDA) to visualise  
200 the distribution of pollen species and sampling sites along the climatic gradients. We  
201 used the variance inflation factor (VIF) to determine high collinearities within the  
202 model, and stopped adding variables to ensure all VIF values are lower than 20 (ter  
203 Braak and Prentice, 1988; Table 1). All ordination analyses were run using the *rda*  
204 function in the *rioja* package version 0.9–26 (Oksanen et al., 2019) in R, using  
205 square-root transformed modern pollen percentages to optimise the signal-to-noise  
206 ratio (Prentice, 1980).

207 For the fossil pollen dataset obtained from GAH, 22 pollen taxa (those present in at  
208 least 3 samples and with a  $\geq 3\%$  maximum) with square-root transformed percentages  
209 were selected for ordination analyses. The length of the first axis was 1.67 SD,  
210 indicating a principal component analysis (PCA) is suitable to investigate the  
211 relationship between the pollen taxa. PCA was run using the *rda* function in the *vegan*  
212 package (version 2.5-4; Oksanen et al., 2019) in R.

213 In addition, weighted-averaging partial least squares (WA-PLS) was employed to  
214 establish a pollen–climate transfer function using the modern pollen dataset, and to  
215 quantitatively reconstruct past climate for the GAH pollen record. More details of the  
216 reconstruction are presented in the Supplement.

217 **Table 1.** Summary statistics for redundancy analysis (RDA) with 19 pollen taxa and four climate  
218 variables. VIF: variance inflation factor;  $P_{\text{ann}}$ : mean annual precipitation (mm);  $M_{\text{co}}$ : mean



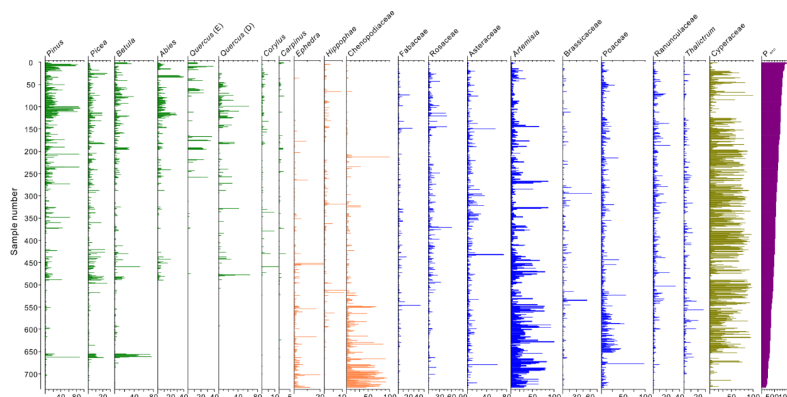
219 temperature of the coldest month (°C); Mt<sub>wa</sub>: mean temperature of the warmest month (°C); T<sub>ann</sub>:  
 220 mean annual temperature (°C); and Elev: elevation (m a.s.l).

Climate variables	VIF (without T <sub>ann</sub> )	VIF (add T <sub>ann</sub> )	Climate variables as sole predictor		Marginal contribution based on climate variables		
			Explained (%)	variance	Explained (%)	variance	<i>p</i> -value
P <sub>ann</sub>	3.0	3.1	5.2		7.1		0.001
Mt <sub>co</sub>	4.5	133.6	4.9		0.3		0.001
Mt <sub>wa</sub>	6.5	111.7	3.7		5.7		0.001
Elev	2.5	3.0	4.5		0.2		0.001
T <sub>ann</sub>	-	403.9	-		-		-

221 **4 Results**

222 *4.1 Relationships of pollen taxa to climatic variables and elevation*

223 The modern pollen dataset for the east Tibetan Plateau contains 107 pollen taxa and  
 224 covers a long P<sub>ann</sub> gradient (161–963 mm) and broad Mt<sub>wa</sub> gradient (1.8–18.5 °C) (Fig.  
 225 2; A1). High abundances of arboreal pollen taxa occur in areas with warm and wet  
 226 climate, for instance, *Abies*, *Quercus* (evergreen, E), *Corylus*, and *Carpinus* are  
 227 mainly distributed in regions with high P<sub>ann</sub> and Mt<sub>co</sub> (Fig. 2; A1). Although high  
 228 abundances of *Pinus*, *Picea*, and *Betula* are also restricted to warm and wet areas,  
 229 they are widely distributed and appear even in extreme drought sampling sites (Fig. 2).  
 230 Drought-tolerant species such as *Chenopodiaceae* and *Ephedra* are restricted to  
 231 regions with low P<sub>ann</sub> and high Mt<sub>wa</sub>, and they have quite low abundances in wet areas  
 232 (Fig. 2).

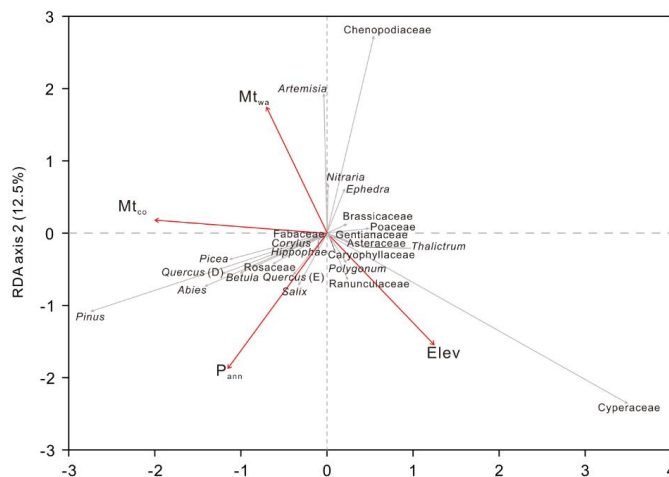


233  
 234 **Figure 2.** Pollen assemblages of surface sediment samples with annual precipitation (P<sub>ann</sub>) from



235 the eastern Tibetan Plateau.

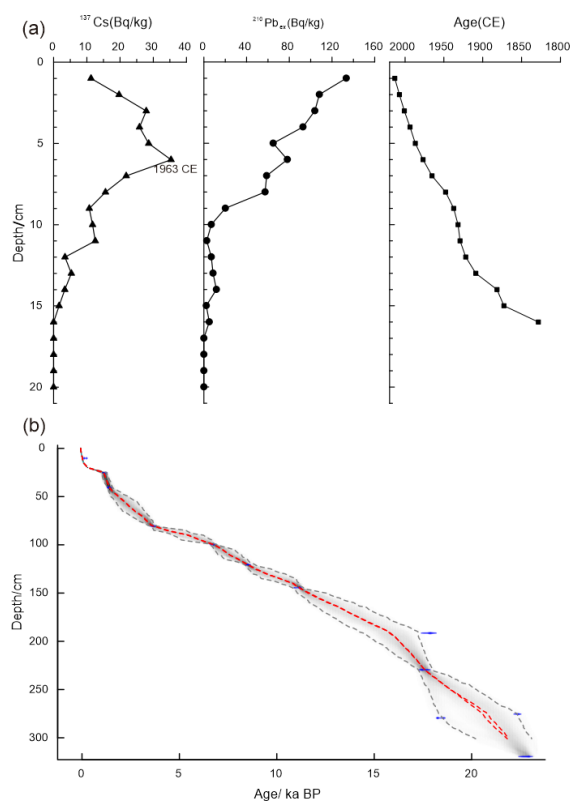
236 Redundancy analysis shows that the first two axes explain 28% of the pollen data  
 237 (axis 1: 15.5%; axis 2: 12.5%; Fig. 3). Arboreal pollen taxa are located in the left of  
 238 the biplot and are positively correlated with  $P_{ann}$  and  $Mt_{co}$ . Asteraceae, Poaceae,  
 239 *Thalictrum*, Ranunculaceae, Caryophyllaceae, and Cyperaceae show a negative  
 240 relationship with  $Mt_{wa}$  and  $Mt_{co}$  while positive with Elev, and are situated in the lower  
 241 right of the biplot. Drought-tolerant pollen including Chenopodiaceae, *Artemisia*, and  
 242 *Ephedra* are situated at the upper right of the biplot, showing positive correlations  
 243 with temperature variables and negative correlations with precipitation (Fig. 3).



244  
 245 **Figure 3.** Redundancy analysis (RDA) of modern pollen samples along with three climate  
 246 variables and elevation.

247 *4.2 Sedimentary lithology and chronology*

248 The sedimentary lithology of the GAH core is comprised of black silt in the upper  
 249 part (0–99 cm), brown clay in the central part (99–240 cm), and dark-brown fine silt  
 250 in the lower part (240–329 cm; Fig. 4). Our study concentrates on the vegetation and  
 251 environment evolution of the upper 176 cm due to the extremely low pollen  
 252 concentrations in the lower part, insufficient for statistical analyses.



253

254 **Figure 4.** Age-depth model of the Gahai Lake sediment core derived from  $^{137}\text{Cs}$ ,  $^{210}\text{Pb}$ , and  $^{14}\text{C}$   
 255 dating. (a) Black line with triangles:  $^{137}\text{Cs}$  age; black line with solid circles:  $^{210}\text{Pb}$ : $^{210}\text{Pb}_{\text{ex}}$  age;  
 256 black line with squares: mean age based on annual lamination counting. (b) Age-depth curve  
 257 based on a  $^{210}\text{Pb}$  profile of recent sediments and 13 AMS radiocarbon dates from Gahai Lake. The  
 258 range of the two grey dashed lines indicate the 95% confidence intervals, and the red dashed lines  
 259 show the single “best” model based on the weighted mean age for each depth.

260 The chronology of the upper 20 cm sediment is established by the  $^{210}\text{Pb}$ -CRS model,  
 261 with dates falling between 1828 and 2013 CE. The AMS  $^{14}\text{C}$  ages of GAH exhibit a  
 262 linear regression with depth, and the ages of the upper 20 cm are calculated based on  
 263 their relationship (Table 2). The age difference between  $^{14}\text{C}$  and  $^{210}\text{Pb}$  of the same  
 264 depth is considered as the reservoir age. We selected two depths (6 cm and 10 cm) to  
 265 calculate an average to reduce errors and obtained a reservoir age of 483 years. The  
 266 age-depth model suggests that the basal age of GAH is about 24 ka BP, and the



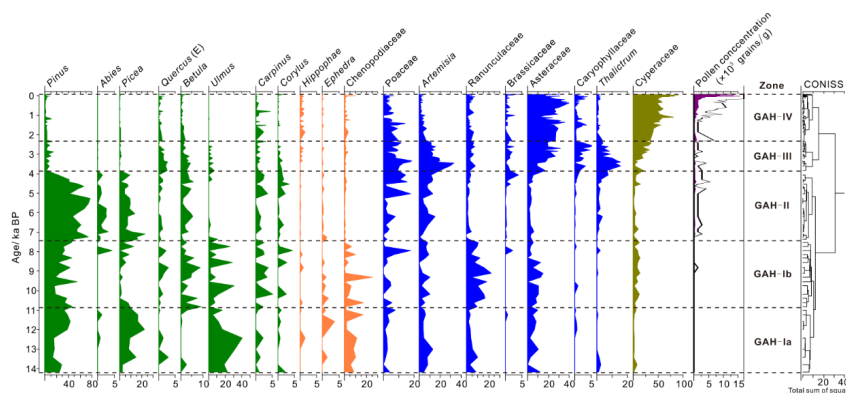
267 sedimentation rate is relatively stable (Fig. 4).

268 **Table 2.** AMS radiocarbon dates for Gahai Lake

Lab ID	Depth (cm)	$\delta^{13}\text{C}$ (‰)	$^{14}\text{C}$ age (yr BP)	Error ( $\pm$ yr)
Beta-546102	10	-25.6	440	30
Beta-546103	25	-25.1	1740	30
Beta-539751	40	-25.7	1960	30
Beta-539752	80	-24.8	3880	30
Beta-546104	99	-24.3	6390	30
Beta-539753	120	-22.1	8180	40
Beta-546105	144	-22.9	10240	30
Beta-575823	191	-24.4	15070	40
Beta-546120	229	-25.4	14870	50
Beta-550230	275	-23.5	18930	60
Beta-546121	279	-22.6	15550	50
Beta-546122	319	-20.5	19440	70

269 *4.3 Pollen record of GAH since the last deglacial*

270 In our study, 52 pollen taxa were identified in the 111 samples from the upper part of  
 271 GAH (0–176 cm), with Cyperaceae, *Pinus*, Asteraceae, and *Artemisia* as dominant  
 272 taxa, while Poaceae, Ranunculaceae, *Ulmus*, and *Picea* are common taxa. The pollen  
 273 record can be demarcated into four zones (Fig. 5). Pollen concentration is extremely  
 274 low (mean 33.5 grains/g) before 7.4 ka BP, and the pollen spectra are dominated by  
 275 arboreal pollen taxa including *Pinus*, *Picea*, *Ulmus*, and *Betula*, together with  
 276 abundant drought-tolerant pollen taxa (such as Chenopodiaceae and *Ephedra*). Pollen  
 277 concentration increases remarkably after 7.4 ka BP, and drought-tolerant pollen taxa  
 278 decrease while *Pinus* increases in the pollen spectra. Between 7.4 and 2.3 ka BP,  
 279 *Pinus* and *Picea* decrease sharply, while *Artemisia*, Poaceae, Asteraceae, and  
 280 *Thalictrum* increase significantly. Pollen concentration increases greatly and the pollen  
 281 spectra are dominated by Cyperaceae after 2.3 ka BP. Cyperaceae rises sharply and  
 282 becomes overwhelmingly dominant in the pollen spectra, and the pollen concentration  
 283 also increases strongly in the last 0.24 ka BP (Fig. 5).

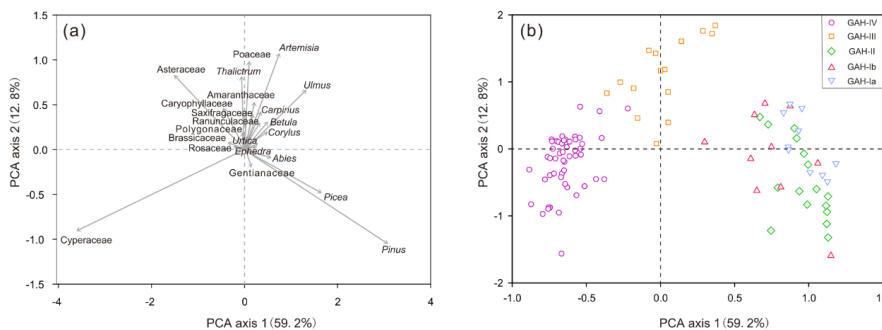


284

285 **Figure 5.** Pollen diagram of the main fossil pollen taxa in Gahai Lake, north-east Tibetan Plateau.

286 **4.4 PCA results**

287 The first two axes of the principal component analysis (PCA) explain 72% of the total  
 288 pollen data (axis 1: 59.2%; axis 2: 12.8%; Fig. 6a). The PCA divides arboreal pollen  
 289 taxa (such as *Pinus*, *Picea*, *Betula*, *Ulmus*), alpine steppe taxa (including *Artemisia*,  
 290 *Poaceae*, *Asteraceae*), and meadow taxa (*Cyperaceae*) into three clear groups. In  
 291 addition, pollen samples of Zones I and II are consistent with arboreal taxa, pollen  
 292 samples from Zone III contain abundant steppe taxa, while samples in Zone IV are  
 293 dominated by *Cyperaceae* (Fig. 6b).



294

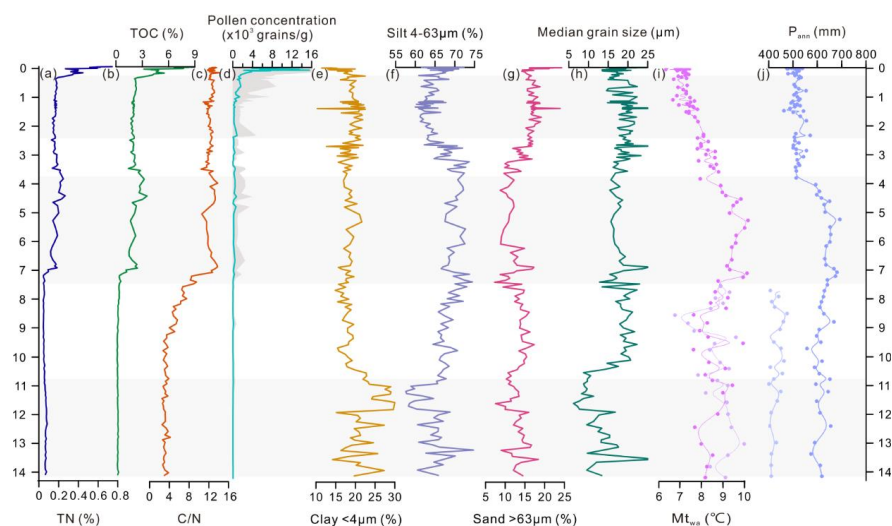
295 **Figure 6.** Principal component analysis (PCA) of fossil pollen taxa (a) and pollen zones (b) from  
 296 Gahai Lake (see Fig. 5 for the pollen zones).



297 *4.5 Sedimentology and conventional geochemistry*

298 The grain-size results of GAH suggest an increasing trend generally which could be  
 299 divided into four stages, with the silt fraction (4–63 μm) accounting for the maximal  
 300 proportion (58–75%; mean 66%) in general (Fig. 7). The clay fraction (<4 μm; 15–  
 301 33%; mean 23%) forms the highest proportion during 14.2–10.8 ka BP, while median  
 302 grain size is very low. The silt fraction increases while the clay fraction decreases  
 303 during 10.8–3.8 ka BP, and the sand fraction (>63 μm) and median grain size first  
 304 increase and then decrease. The sand fraction and median grain size slightly increase  
 305 while the clay fraction tends to decrease after 3.8 ka BP, and the silt fraction increases  
 306 first and then decreases.

307 TOC, TN, and C/N ratios fluctuate greatly since 14.2 ka BP, and TOC and TN present  
 308 simultaneous change trends (Fig. 7). TOC and TN values are remarkably low and C/N  
 309 ratios are lower than 10 between 14.2 and 7 ka BP. TOC, TN, and C/N ratios increase  
 310 significantly and C/N ratios are higher than 10 between 7 and 4 ka BP. TOC, TN, and  
 311 C/N ratios reduce slightly but are still higher than 10 after 4 ka BP. TOC and TN  
 312 values increase drastically while C/N ratios have no obvious change during the last  
 313 0.24 ka BP (since 1710 CE).



314  
 315 **Figure 7.** Comparison of the multi-proxy records from Gahai Lake. (a) Total nitrogen (TN), (b)



316 total organic carbon (TOC), (c) C/N ratio, (d) pollen concentration, (e-h) grain size distribution  
317 and median grain size, (i) quantitative reconstruction of mean temperature of the warmest month  
318 ( $M_{twa}$ ). Purple curve indicates the reconstruction based on the pollen assemblages including the  
319 arboreal pollen and the light purple curve represents the reconstruction based on the pollen  
320 assemblages removing the arboreal pollen (before 7.4 ka only). (j) quantitative reconstruction of  
321 mean annual precipitation ( $P_{ann}$ ). Blue curve is the reconstruction based on the pollen assemblages  
322 including the arboreal pollen and the light blue curve is the reconstruction based on the pollen  
323 assemblages without the arboreal pollen (before 7.4 ka only). The grey shading denotes the  
324 different pollen zones of Gahai Lake.

## 325 **5 Discussion**

### 326 *5.1 Patterns and interpretation of the proxies*

327 TOC is a proxy for the abundance of organic matter which originates from aquatic  
328 organisms and terrestrial vegetation, and TN represents the nutritional conditions of  
329 the lake. C/N ratios are used to trace the plant source of the organic matter. C/N ratios  
330 of the nonvascular aquatic plants and algae are generally between 4 and 10, and C/N  
331 ratios >20 indicate that organic matter mainly originates from terrestrial vascular  
332 plants. Ratios ranging from 10 to 20 suggest that the organic matter is derived from a  
333 mixture of aquatic and terrestrial plants (Meyers and Ishiwatari, 1993; Meyers, 2003;  
334 Kasper et al., 2015).

335 The grain-size composition of lake sediments can be used to trace the source of clastic  
336 particles, aeolian activity, and water-level fluctuations, which reflect the regional  
337 climate conditions (Håkanson and Jansson, 1983; Liu et al., 2016). The sources of  
338 lacustrine sediments include clastic materials carried by inflow rivers, aeolian inputs,  
339 and authigenic chemical deposition (Xiao et al., 2013). Particle-size analyses from  
340 lacustrine sediments and modern surface sediments suggest that the sand fraction (>63  
341  $\mu\text{m}$ ) or particles >50  $\mu\text{m}$  are mainly transported by wind and could be an indicator of  
342 aeolian activity (Qiang et al., 2014; Wang et al., 2015; Liu et al., 2016). Particle-size  
343 variation can reflect changes in water level, with coarser grains indicating a rise in



344 water level as river discharge would need to be greater to transport the heavier grains,  
345 and hence suggesting an increase in precipitation (Håkanson and Jansson, 1983; Liu  
346 et al., 2008). Therefore, we speculate that a high silt fraction (4–63  $\mu\text{m}$ ) in Gahai Lake  
347 reflects an increase in the lake water level, while a high clay fraction ( $<4 \mu\text{m}$ ) content  
348 reflects a low stand. In addition, a high proportion of the sand fraction ( $>63\mu\text{m}$ )  
349 indicates aeolian activity intensity. The variation of the median grain size is consistent  
350 with the sand fraction thus also reflecting aeolian deposition.

### 351 *5.2 Determination of exogenous pollen grains*

352 According to modern pollen research from the Tibetan Plateau and northern China,  
353 *Pinus*, *Picea*, and *Betula* are dominant pollen taxa in forest samples, and these taxa  
354 have a good diffusion capacity and are easily transported for long distances from their  
355 pollen source (Lu et al. 2004; Ma et al., 2008; Ma et al., 2015). *Ulmus* also has a good  
356 diffusion and can spread up to 40 km away, and can therefore be a regional vegetation  
357 component (Xu et al., 2007). The main arboreal pollen taxa in the GAH core are thus  
358 highly diffusive species which may bias the interpretation of the source of arboreal  
359 pollen.

360 The main pollen taxa have notable spatial distribution characteristics owing to their  
361 ecological environment based on modern pollen research and the modern pollen  
362 dataset. Arboreal taxa including *Pinus*, *Picea*, and *Betula* are mainly distributed in a  
363 warm and humid environment (Lu et al., 2004). *Ulmus* is a drought-tolerant and light-  
364 demanding plant which can survive at precipitation levels lower than 200 mm per year  
365 (Shen et al., 2005). Previous modern pollen studies reveal that Chenopodiaceae and  
366 *Ephedra* are commonly found in the desert, indicating a tolerance for dry climatic  
367 conditions (Yu et al., 2001; Huang et al., 2018; Qin et al., 2021); and our modern  
368 pollen dataset for the east Tibetan Plateau suggests that xerophilous taxa such as  
369 *Ephedra* and Chenopodiaceae are restricted to areas with  $P_{\text{ann}}$  lower than 400 mm, and  
370 almost absent in samples with high precipitation (Fig. 2). Fossil pollen spectra from  
371 the Tibetan Plateau with abundant arboreal pollen taxa together with low pollen



372 concentrations are considered to represent extreme arid conditions and sparse  
373 vegetation (Kramer et al., 2010b; Ma et al., 2019). Therefore, we argue that the  
374 arboreal pollen including *Pinus*, *Picea*, and *Ulmus* has been transported by wind from  
375 beyond the watershed, and that the high abundance of drought-tolerant herbaceous  
376 taxa (weak dispersal ability) and low pollen concentrations indicate a sparse  
377 vegetation cover around the lake between 14.2 and 7.4 ka BP, suggesting an extremely  
378 arid climate.

### 379 *5.3 Evolution of vegetation and climate history since the last glacial*

380 Palaeo-vegetation and palaeo-climate is reconstructed based on the fossil pollen, TOC,  
381 TN, C/N ratios, and grain-size record of Gahai Lake since the last deglacial.

382 From 14.2 to 10.8 ka BP, alpine steppe or desert covered the study area with the  
383 arboreal pollen derived from the surrounding mountains in the south-east of the basin.  
384 Pollen-based past  $P_{ann}$  reconstructions are likely to be overestimated since the  
385 exogenous arboreal pollen has not been excluded from the pollen spectra. Remarkably,  
386 however, reconstructed  $Mt_{wa}$  shows no bias from these exogenous arboreal pollen,  
387 thus the climate was probably mild and arid during this period (Fig. 7). Quite low  
388 TOC and TN contents, and C/N ratios below four suggest that the organic matter is  
389 mainly derived from aquatic plants, and also imply low terrestrial biomass  
390 productivity (Fig. 7; Zhu et al., 2015). Clay fraction reaches its maximum value,  
391 reflecting a low water level and weak aeolian activity (Fig. 7). In summary, Gahai was  
392 probably a small and shallow pond under a mild, arid climate during this period, with  
393 the surrounding vegetation dominated by alpine steppe or desert.

394 From 10.8 to 7.4 ka BP, Ranunculaceae and Cyperaceae show a slight increase, and  
395 alpine steppe occurs across the region (Fig. 5). The reconstruction suggests that  $Mt_{wa}$   
396 decreases compared with the former stage, whereas reconstructed  $P_{ann}$  still reflects the  
397 exaggerated contribution of exogenous arboreal pollen (Fig. 7). TOC and C/N ratios  
398 rise during the early Holocene, implying an increase in biological productivity  
399 although still mainly from aquatic plants (Fig. 7). The silt and sand fractions and



400 median grain size significantly increase, while the clay fraction decreases sharply,  
401 indicating that the water level rose and that aeolian activity strengthened during the  
402 early Holocene (Fig. 7). Therefore, we infer that the Gahai Basin had a cold and arid  
403 climate with enhanced wind strength during the early Holocene, and an alpine steppe  
404 vegetation while the lake had an increased water level.

405 The pollen concentration, silt fraction, TOC, and TN remarkably increase, and C/N  
406 ratios above 10 suggest that the climate and vegetation greatly improved after 7.4 ka  
407 BP to reach an optimum. Gahai Lake was at a high stand with increased terrestrial  
408 organic matter input (Fig. 7). We infer that Gahai Lake grew from a small pond and  
409 that the pollen spectra mainly reflect vegetation change within the catchment, with the  
410 reconstructed  $P_{ann}$  and  $Mt_{wa}$  reflecting the regional climate variation with weak  
411 influence from exogenous pollen during the mid-Holocene (Fig. 7). The pollen  
412 spectra are dominated by *Pinus* and *Picea* while drought-tolerant taxa (such as  
413 *Chenopodiaceae* and *Ephedra*) have a low abundance, indicating a vegetation shift  
414 from alpine steppe to montane forest between 7.4 and 3.8 ka BP (Ma et al., 2008;  
415 Zhao et al., 2009), under a warm and wet climate ( $P_{ann}$  and  $Mt_{wa}$  reach their peaks; Fig.  
416 7). In addition, the sand fraction and median grain size slightly decline suggesting  
417 weaker aeolian activity during this period (Fig. 7).

418 During 3.8 to 2.3 ka BP, the pollen spectra are characterised by a high percentage of  
419 Poaceae, *Artemisia*, and Asteraceae (major component of alpine steppe), and arboreal  
420 pollen taxa, especially *Pinus* and *Picea*, sharply decrease, indicating the tree-line  
421 retreated to a lower elevation and a shift in vegetation type to alpine steppe  
422 (Herzschuh et al., 2010; Shen et al., 2021; Fig. 5). Reconstructed  $P_{ann}$  and  $Mt_{wa}$   
423 decrease significantly, suggesting mild and arid climatic conditions (Fig. 7). TOC, TN,  
424 and C/N ratios slightly decrease compared with the previous stage, suggesting the  
425 weakened input of organic matter although the source remains unchanged (Fig. 7).  
426 The silt fraction substantially decreases while the sand fraction and median grain size  
427 have an increasing trend, suggesting weaker hydrodynamic conditions and  
428 strengthened aeolian activity (Fig. 7). In brief, the climate turned mild and arid and



429 aeolian activity strengthened. Alpine steppe dominated across the region during this  
430 period.

431 From 2.3 to 0.24 ka BP, the dominant taxa change from alpine steppe (Poaceae,  
432 *Artemisia*, and Asteraceae) components (Ma et al., 2015; Qin et al., 2021) to alpine  
433 meadow (Cyperaceae) (Herzschuh et al., 2007; 2010; Fig. 5), and  $Mt_{wa}$  reconstruction  
434 reveals a cold environment (Fig. 7). TOC, TN, and C/N ratios suggest the total  
435 biogenic productivity input and its source has little changed compared with the  
436 previous stage (Fig. 7). Silt fraction decreases while the sand fraction and median  
437 grain size increase, indicating weaker water dynamics and enhanced aeolian activity.

438 After 0.24 ka BP (1710 CE), the pollen spectra are dominated by Cyperaceae  
439 (maximum, 95%; Fig. 5). Previous vegetation investigations suggest that overgrazing  
440 causes the proportion of Cyperaceae to increase and become the dominant taxon, and  
441 thus could be an indicator of human activities (Yuan et al., 2004; Dong et al., 2004;  
442 Miehle et al., 2014; Lin et al., 2016). Hence the vegetation during this period could  
443 have been disturbed by human activities. In addition, TOC, TN, and pollen  
444 concentration notably increase, indicating terrestrial material input strengthened,  
445 possibly as a result of increased surface erosion (silt fraction increases; Fig. 7) due to  
446 the destruction of vegetation by human activities.

#### 447 *5.4 Comparison of the regional climate and vegetation records from the north-east* 448 *Tibetan Plateau in the early Holocene*

449 Climate and vegetation as revealed by pollen records covering the early Holocene on  
450 the north-east Tibetan Plateau are inconsistent, which may be due to the following  
451 reasons: local factors have a greater effect than regional climate (Chen et al., 2020);  
452 the distance of sampling sites from forested areas affects the results of vegetation  
453 reconstruction (Sun et al., 2017); and different climatic factors influence the regional  
454 vegetation distribution of the eastern Tibetan Plateau (Zhao et al., 2011). Based on the  
455 results of TOC, TN, grain size, and pollen analysis, we infer that Gahai Lake was  
456 surrounded by alpine steppe vegetation under cool and arid climatic conditions, and



457 that the arboreal pollen was mainly transported by wind from the surrounding  
458 mountains during the early Holocene. Other records from the north-east Tibetan  
459 Plateau confirm these general features of climate and vegetation during the early  
460 Holocene. For example, results from an adjacent peatland show that the climate and  
461 vegetation of the Zoige Basin and Nianbaoyeze Mountains reached their optimum  
462 during the mid-Holocene and had a cooler temperature and lower humidity during the  
463 early Holocene (Zhou et al., 2010; Zhao et al., 2011; Sun et al., 2017; Herzschuh et al.,  
464 2014). A reconstruction from Hurleg Lake also indicates that it was at a low stand  
465 during the early Holocene and that the vegetation type was desert or desert steppe  
466 (Zhao et al., 2007; Fan et al., 2014). Cheng et al. (2009) analyse the pollen record of  
467 Dalianhai Lake (from 16 ka BP) and conclude that this region had a dry climate and  
468 was covered by steppe desert during the early Holocene. Multi-proxy records from  
469 Qinghai Lake including pollen, carbonate, TOC, TN,  $\delta^{13}\text{C}$  of organic matter (Shen et  
470 al., 2005), redness records (Ji et al., 2005), and lake level (Liu et al., 2015) reveal that  
471 this region had a dry climate and weak East Asian summer monsoon (Chen et al.,  
472 2016). Similar records are found from Koucha Lake (Herzschuh et al., 2009), Kuhai  
473 Lake (Wischniewski et al., 2011), Luanhaizi Lake (Herzschuh et al., 2005; 2010), and  
474 the arid region of central Asian moisture variation based on eleven records integrated  
475 during the early Holocene. (Chen et al., 2008; 2020). The pollen assemblages of  
476 Donggi Cona Lake show a high percentage of *Ephedra*, which suggests an arid  
477 environment in the early Holocene, although the quantitative reconstruction shows  
478 this period was the wettest stage in the Holocene (Tian et al., 2014; Huang et al.,  
479 2018). Based on the above investigations, we can conclude that the climate was arid  
480 on the north-east Tibetan Plateau during the early Holocene.

481

## 482 **6. Conclusions**

483 Based on modern pollen investigations for the east Tibetan Plateau, arboreal pollen  
484 can be determined as exogenous taxa when they appear together with drought-tolerant



485 taxa and low pollen concentrations in fossil pollen spectra. The Gahai Basin was  
486 covered by the alpine steppe or desert under a cold and dry climate during 14.2–7.4 ka  
487 BP; montane forest migrated into the basin and the climate reached an optimum  
488 between 7.4 and 3.8 ka BP according to the evidence of TN, TOC, C/N, and grain-size  
489 records; the vegetation reverted to alpine steppe owing to a drying climate during 3.8  
490 and 2.3 ka BP, after which steppe was replaced by alpine meadow as the climate  
491 cooled. In addition, the vegetation showed signs of being influenced by human  
492 activity during the last 0.24 ka BP.

493

494 **Data availability.** The data used in this study can be obtained from the corresponding  
495 author Xianyong Cao (xcao@itpcas.ac.cn).

496

497 **Author contribution.** NW extracted and identified pollen samples, analyzed pollen  
498 data and wrote manuscript; LL, XH, and YZ participated in sample collecting and  
499 data analysis; HW contributed to the detailed comments; XC designed this study and  
500 led interpretation. All authors commented and improved manuscript.

501

502 **Competing interests.** The authors declare that they have no conflict of interest.

503

504 **Acknowledgements.** This study was supported by the Basic Science Center for  
505 Tibetan Plateau Earth System (BSCTPES, NSFC project No. 41988101), the National  
506 Natural Science Foundation of China (Grant No. 41877459) and CAS Pioneer  
507 Hundred Talents Program (Xianyong Cao). We thank Cathy Jenks for help with  
508 language editing.

## 509 **References**

510 An, Z., Colman, S.M., Zhou, W., Li, X., Brown, E.T., Jull, A.J.T., Cai, Y., Huang, Y.,  
511 Lu, X. F., Chang, H., Song, Y. G., Sun, Y. B., Xu, H., Liu, W. G., Jin, Z. D., Liu, X.  
512 D., Cheng, P., Liu, Y., Ai, L., Li, X., Liu, X., Yan, L., Shi, Z., Wang, X., Wu, F.,



- 513 Qiang, X. K., Dong, J., Lu, F., and Xu, X.: Interplay between the westerlies and  
514 Asian monsoon recorded in Lake Qinghai sediments since 32 ka. *Sci. Rep.* 2, 619,  
515 doi: 10.1038/srep00619, 2012.
- 516 Andersen, K. K., Azuma, N., Barnola, J. M., Bigler, M., Biscaye, P., Caillon, N.,  
517 Chappellaz, J., Clausen, H. B., DahlJensen, D., Fischer, H., Fluckiger, J., Fritzsche,  
518 D., Fujii, Y., Goto-Azuma, K., Gronvold, K., Gundestrup, N. S., Hansson, M.,  
519 Huber, C., Hvidberg, C. S., Johnsen, S. J., Jonsell, U., Jouzel, J., Kipfstuhl, S.,  
520 Landais, A., Leuenberger, M., Lorrain, R., Masson-Delmotte, V., Miller, H.,  
521 Motoyama, H., Narita, H., Popp, T., Rasmussen, S. O., Raynaud, D., Rothlisberger,  
522 R., Ruth, U., Samyn, D., Schwander, J., Shoji, H., Siggard-Andersen, M. L.,  
523 Steffensen, J. P., Stocker, T., Sveinbjornsdottir, A. E., Svensson, A., Takata, M.,  
524 Tison, J. L., Thorsteinsson, T., Watanabe, O., Wilhelms, F., and White, J. W. C.:  
525 High-resolution record of Northern Hemisphere climate extending into the last  
526 interglacial period, *Nature*, 431, 147–151, doi: 10.1038/nature02805, 2004.
- 527 Birks, H. J. B.: Contributions of Quaternary botany to modern ecology and  
528 biogeography, *Plant. Ecol. Diversity.*, 12, 189–385, doi:  
529 10.1080/17550874.2019.1646831, 2019.
- 530 Blaauw, M., and Christen, J. A.: Flexible paleoclimate age-depth models using an  
531 autoregressive gamma process, *Bayesian. Anal.*, 6: 457–474, doi:  
532 10.1214/ba/1339616472, 2011.
- 533 Blaauw, M., Christen, J. A., Aquino Lopez, M. A., Esquivel Vazquez, J., Gonzalez V.  
534 O. M., Belding, T., Theiler, J., Gough, B., and Karney, C.: rbacon: age-depth  
535 modelling using Bayesian statistics, <https://cran.r-project.org/web/packages/rbacon/index.html>. Accessed Jan 2020, 2021.
- 537 Bryson, R. A.: Airstream climatology of Asia. *Proceedings of International*  
538 *Symposium on the Qinghai-Xizang Plateau and Mountain Meteorology*. American  
539 *Meteorological Society*, Boston, MA, pp. 604–617, 1986.
- 540 Cai, M., Fang, X., Wu, F., Miao, Y., and Appel, E.: Pliocene-Pleistocene stepwise  
541 drying of Central Asia: Evidence from paleomagnetism and sporopollen record of



- 542 the deep borehole SG-3 in the western Qaidam Basin, NE Tibetan Plateau, Global  
543 Planet. Change., 94–95, 72–81, doi: 10.1016/j.gloplacha.2012.07.002, 2012.
- 544 Cao, X., Tian, F., Telford, R. J., Ni, J., Xu, Q., Chen, F., Liu, X., Stebich, M., Zhao, Y.,  
545 and Herzschuh, U.: Impacts of the spatial extent of pollen-climate calibration-set on  
546 the absolute values, range and trends of reconstructed Holocene precipitation. *Quat.*  
547 *Sci. Rev.* 178, 37–53, doi: 10.1016/j.quascirev.2017.10.030, 2017.
- 548 Chen, F., Dong, G., Zhang, D., Liu, X., Jia, X., An, C., Ma, M., Xie, Y., Barton, L.,  
549 Ren, X., Zhao, Z., Wu, X., and Jones, M. K.: Agriculture facilitated permanent  
550 human occupation of the Tibetan Plateau after 3600 B.P., *Science*, 347, 248–250,  
551 doi: 10.1126/science.1259172, 2015.
- 552 Chen, F., Wu, D., Chen, J., Zhou, A., Yu, J., Shen, J., Wang, S., and Huang, X.:  
553 Holocene moisture and East Asian summer monsoon evolution in the north-eastern  
554 Tibetan Plateau recorded by Lake Qinghai and its environs: a review of conflicting  
555 proxies. *Quat. Sci. Rev.* 154, 111–129, doi: 10.1016/j.quascirev.2016.10.021, 2016.
- 556 Chen, F., Yu, Z., Yang, M., Ito, E., Wang, S., Madsen, D. B., Huang, X., Zhao, Y., Sato,  
557 T., Birks, H. J. B., Boomer, I., Chen, J., An, C., and Wünnemann, B.: Holocene  
558 moisture evolution in arid central Asia and its out-of-phase relationship with Asian  
559 monsoon history. *Quat. Sci. Rev.* 27, 351–364, doi:  
560 10.1016/j.quascirev.2007.10.017, 2008.
- 561 Chen, F., Zhang, J., Liu, J., Cao, X., Hou, J., Zhou, L., Xu, X., Liu, X., Wang, M., Wu,  
562 D., Huang, L., Zeng, T., Zhang, S., Huang, W., Zhang, X., and Yang, K.: Climate  
563 change, vegetation history, and landscape responses on the Tibetan Plateau during  
564 the Holocene: A comprehensive review. *Quat. Sci. Rev.*, 243, 106444, doi:  
565 10.1016/j.quascirev.2020.106444, 2020.
- 566 Cheng, B., Chen, F., and Zhang, J.: Palaeovegetational and palaeoenvironmental  
567 changes since the last deglacial in Gonghe Basin, northeast Tibetan Plateau, *J.*  
568 *Geogr. Sci.* 23, 136–146, doi: 10.1007/s11442-013-0999-5, 2013.
- 569 Chevalier, M., Davis, B. A. S., Heiri, O., Seppä, H., Chase, B. M., Gajewski, K.,  
570 Lacourse, T., Telford, R. J., Finsinger, W., Guiot, J., Kühl, N., Maezumi, S. Y.,



- 571 Tipton, J. R., Carter, V. A., Brussel, T., Phelps, L. N., Dawson, A., Zanon, M., Vallé,  
572 F., Nolan, C., Mauri, A., de Vernal, A., Izumi, K., Holmström, L., Marsicek, J.,  
573 Goring, S., Sommer, P. S., Chaput, M., and Kupriyanov, D.: Pollen-based climate  
574 reconstruction techniques for late Quaternary studies, *Earth-Sci. Rev.* 210, 103384,  
575 doi: 10.1016/j.earscirev.2020.103384, 2020.
- 576 Du, Y.: Land cover of Tibet Plateau (2015), National Tibetan Plateau Data Center,  
577 2019.
- 578 Duan, Y., Zhao, Y., Wu, Y., He, J., Xu, L., Zhang, X., Ma, L., and Qian, R.:  $\delta D$  values  
579 of n-alkanes in sediments from Gahai Lake, Gannan, China: implications for  
580 sources of organic matter, *J. Paleolimnol.* 56, 95–107, doi: 10.1007/s10933-016-  
581 9895-1, 2016.
- 582 Dykoski, C. A., Edwards, R. L., Cheng, H., Yuan, D. X., Cai, Y., Zhang, M., Lin, Y.,  
583 Qing, J., An, Z., and Revenaugh, J.: A high-resolution, absolute-dated Holocene and  
584 deglacial Asian monsoon record from Dongge Cave, China, *Earth Planet. Sci. Lett.*,  
585 233, 71–86, doi: 10.1016/j.epsl.2005.01.036, 2005.
- 586 Fan, Q., Ma, H., Wei, H., and An, F.: Holocene lake-level changes of Hurleg Lake on  
587 northeastern Qinghai-Tibetan Plateau and possible forcing mechanism, *Holocene*,  
588 24, 274–283, doi:10.1177/0959683613517399, 2014.
- 589 Fægri, K., and Iversen, J.: Textbook of pollen analysis, Munksgaard, Copenhagen,  
590 1975.
- 591 Håkanson, L., and Jansson, M.: Principles of Lake Sedimentology, Springer, 316 pp.
- 592 Herzschuh, U.: Reliability of pollen ratios for environmental reconstructions on the  
593 Tibetan Plateau, *J. Biogeogr.* 34, 1265–1273, doi: 10.1111/j.1365-  
594 2699.2006.01680.x, 2007.
- 595 Herzschuh, U., Birks, H. J. B., Mischke, S., Zhang, C., and Böhner, J.: A modern  
596 pollen-climate calibration set based on lake sediments from the Tibetan Plateau and  
597 its application to a Late Quaternary pollen record from the Qilian Mountains, *J.*  
598 *Biogeogr.* 37, 752–766, doi: 10.1111/j.1365-2699.2009.02245.x, 2010.
- 599 Herzschuh, U., Borkowski, J., Schewe, J., Mischke, S., and Tian, F.: Moisture



600 advection feedback supports strong early-to-mid Holocene monsoon climate on the  
601 eastern Tibetan Plateau as inferred from a pollen-based reconstruction, *Paleogeogr.*  
602 *Paleoclimatol. Paleoecol.* 402, 44–54, doi: 10.1016/j.palaeo.2014.02.022, 2014.

603 Herzsuh, U., Kramer, A., Mischke, S., and Zhang, C.: Quantitative climate and  
604 vegetation trends since the late glacial on the north-east Tibetan Plateau deduced  
605 from Koucha Lake pollen spectra, *Quat. Res.* 71, 162–171, doi:  
606 10.1016/j.yqres.2008.09.003, 2009.

607 Herzsuh, U., Kürschner, H., and Mischke, S.: Temperature variability and vertical  
608 vegetation belt shifts during the last ~50,000 yr in the Qilian Mountains (NE  
609 margin of the Tibetan Plateau, China), *Quat. Res.*, 66, 133–146, doi:  
610 10.1016/j.yqres.2006.03.001, 2006.

611 Herzsuh, U., Winter, K., Wünnemann, B., and Li, S.: A general cooling trend on the  
612 central Tibetan Plateau throughout the Holocene recorded by the Lake Zigetang  
613 pollen spectra, *Quat. Int.*, 154–155, 113–121, doi: 10.1016/j.quaint.2006.02.005,  
614 2006.

615 Herzsuh, U., Zhang, C., Mischke, S., Herzsuh, R., Mohammadi, F., Mingram, B.,  
616 Kürschner, H., and Riedel, F.: A late Quaternary lake record from the Qilian  
617 Mountains (NW China), evolution of the primary production and the water depth  
618 reconstructed from macrofossil, pollen, biomarker and isotope data, *Global Planet.*  
619 *Change*, 46, 361–379, doi: 10.1016/j.gloplacha.2004.09.024, 2005.

620 Hill, M. O., and Gauch, H. G.: Detrended correspondence analysis: an improved  
621 ordination technique, *Vegetatio*, 42, 41–58, <https://doi.org/10.1007/BF00048870>,  
622 1980.

623 Huang, X., Liu, S., Dong, G., Qiang, M., Bai, Z., Zhao, Y., and Chen, F.: Early human  
624 impacts on vegetation on the north-east Qinghai-Tibetan Plateau during the middle  
625 to late Holocene. *Prog. Phys. Geogr.* 41, 1–16, doi: 10.1177/0309133317703035,  
626 2017.

627 Huang, X., Peng, W., Rudaya, N., Grimm, E. C., Chen, X., Cao, X., Zhang, J., Pan, X.,  
628 Liu, S., Chen, C., and Chen, F.: Holocene Vegetation and Climate Dynamics in the



- 629 Altai Mountains and Surrounding Areas, *Geophys. Res. Lett.*, 45, 6628–6636. doi:  
630 10.1029/2018GL078028, 2018
- 631 Ji, J., Shen, J., Balsam, W., Chen, J., Liu, L., and Liu, X.: Asian monsoon oscillations  
632 in the north-east Qinghai-Tibet Plateau since the late glacial as interpreted from  
633 visible reflectance of Qinghai Lake sediments, *Earth Planet. Sci. Lett.*, 233, 61–70,  
634 doi: 10.1016/j.epsl.2005.02.025, 2005.
- 635 Juggins, S., 2012. Rioja: analysis of Quaternary science data version 0.7-3. Available  
636 at: <http://cran.r-project.org/web/packages/rioja/index.html>.
- 637 Juggins, S., and Birks, H. J. B.: Quantitative environmental reconstructions from  
638 biological data, in: Birks, H. J. B., Lotter, A. F., Juggins, S., and Smol, J. P.,  
639 Tracking environmental change using lake sediments (vol. 5): Data handling and  
640 numerical techniques, Springer, Netherlands, 431–494, doi: 10.1007/978-94-007-  
641 2745-8, 2012.
- 642 Kasper, T., Habertzettl, T., Wang, J., Daut, G., Doberschütz, S., Zhu, L., and  
643 Mäusbacher, R.: Hydrological variations on the Central Tibetan Plateau since the  
644 LGM and their teleconnections to inter-regional and hemispheric climate variations.  
645 *J. Quat. Sci.* 30, 70–78, doi: 10.1002/jqs.2759, 2015.
- 646 Kramer, A., Herzsuh, U., Mischke, S., and Zhang, C.: Holocene tree-line shifts and  
647 monsoon variability in the Hengduan Mountains (south-eastern Tibetan Plateau)  
648 implications from palynological investigations. *Palaeogeogr. Palaeoclimatol.*  
649 *Palaeoecol.* 286, 23–41, doi: 10.1016/j.palaeo.2009.12.001, 2010a.
- 650 Kramer, A., Herzsuh, U., Mischke, S., and Zhang, C.: Late Glacial vegetation and  
651 climate oscillations on the south-eastern Tibetan Plateau inferred from the Lake  
652 Naleng pollen profile. *Quat. Res.* 73, 324–335, doi: 10.1016/j.yqres.2009.12.003,  
653 2010b.
- 654 Li, K., Liao, M., Ni, J., Liu, X., and Wang, Y.: Treeline composition and biodiversity  
655 change on the southeastern Tibetan plateau during the past millennium, inferred  
656 from a high-resolution alpine pollen record. *Quat. Sci. Rev.*, 206, 44–55, doi:  
657 10.1016/j.quascirev.2018.12.029, 2019.



- 658 Li, Q., Ge, Q., and Tong, G.: Modern pollen-vegetation relationship based on  
659 discriminant analysis across an altitudinal transect on Gongga Mountain, eastern  
660 Tibetan Plateau, *Chin. Sci. Bull.*, 57, 4600–4608, doi: 10.1007/s11434-012-5236-6,  
661 2012.
- 662 Li, Y., Qiang, M., Huang, X., Zhao, Y., Leppänen, J. J., Weckström, J., and Välranta,  
663 M.: Lateglacial and Holocene climate change in the NE Tibetan Plateau:  
664 Reconciling divergent proxies of Asian summer monsoon variability. *Catena*, 199,  
665 105089, doi: 10.1016/j.catena.2020.105089, 2021.
- 666 Liang, C., Zhao, Y., Qin, F., Zheng, Z., Xiao, X., Ma, C., Li, H., and Zhao, W.: Pollen-  
667 based Holocene Quantitative Temperature Reconstruction on the Eastern Tibetan  
668 Plateau Using a Comprehensive Method Framework, *Sci. China. Earth. Sci.*, 63,  
669 1144–1160, doi: 10.1007/s11430-019-9599-y, 2020.
- 670 Liang, W.: *Luqu County Annals*. Gansu Culture Press, Lanzhou, 2006. (in Chinese)
- 671 Liu, S., Kruse, S., Scherler, D., Ree, R. H., Zimmermann, H. H., Stoof-Leichsenring,  
672 K. R., Epp, L. S., Mischke, S., and Herzsuh, U.: Sedimentary ancient DNA  
673 reveals a threat of warming-induced alpine habitat loss to Tibetan Plateau plant  
674 diversity, *Nat. Commun.*, 12, 2995, doi: 10.1038/s41467-021-22986-4, 2021.
- 675 Liu X., Lai Z., Madsen D., and Zeng, F.: Last deglacial and Holocene lake level  
676 variations of Qinghai Lake, north-east Qinghai-Tibetan Plateau, *J. Quat. Sci.*, 30,  
677 245-257, doi: 10.1002/jqs.2777, 2015.
- 678 Liu, X., Herzsuh, U., Shen, J., Jiang, Q., and Xiao, X.: Holocene environmental and  
679 climatic changes inferred from Wulungu Lake in northern Xinjiang, China, *Quat.*  
680 *Res.*, 70, 412–425, doi: 10.1016/j.yqres.2008.06.005, 2008.
- 681 Liu, X., Vandenberghe, J., An, Z., Li, Y., Jin, Z., Dong, J., and Sun, Y.: Grain size of  
682 Lake Qinghai sediments: implications for riverine input and Holocene monsoon  
683 variability, *Palaeogeogr. Palaeoclimatol. Palaeoecol.* 449, 41–51, doi:  
684 10.1016/j.palaeo.2016.02.005, 2016.
- 685 Lowe, J. J., and Walker, M. J. C.: *Reconstructing Quaternary Environments*, Harlow:  
686 Longman, 1–472, 1997.



- 687 Lu, H., Wang S., Shen, C., Yang, X., Tong, G., and Liao, G.: Spatial pattern of modern  
688 *Abies* and *Picea* pollen in the Qinghai-Xizang Plateau. *Quat. Sci.* 24, 39–49, (in  
689 Chinese with English abstract).
- 690 Luo, C., Zheng, Z., Tarasov, P., Pan, A., Huang, K. Y., Beaudouin, C., and An, F.:  
691 Characteristics of the modern pollen distribution and their relationship to vegetation  
692 in the Xinjiang region, northwestern China, *Rev. Palaeobot. Palynol.* 153, 282–295,  
693 doi: 10.1016/j.revpalbo.2008.08.007, 2009.
- 694 Ma, Q., Zhu, L., Lü, X., Wang, J., Ju, J., Kasper, T., Daut, G., and Haberzettl, T.: Late  
695 glacial and Holocene vegetation and climate variations at Lake Tangra Yumco,  
696 central Tibetan Plateau, *Global Planet. Change.*, 174, 16–25, doi:  
697 10.1016/j.gloplacha.2019.01.004, 2019a.
- 698 Ma, Q., Zhu, L., Lu, X., Wang, Y., Guo, Y., Wang, J., Ju, J., Peng, P., and Tang, L.:  
699 Modern pollen assemblages from surface lake sediments and their environmental  
700 implications on the southwestern Tibetan Plateau, *Boreas*, 46, 242–253, doi:  
701 10.1111/bor.12201, 2017.
- 702 Ma, Q., Zhu, L., Wang, J., Ju, J., Wang, Y., Lü, X., Kasper, T., and Haberzettl, T.: Late  
703 Holocene vegetation responses to climate change and human impact on the central  
704 Tibetan Plateau, *Sci. Total Environ.* 708, 135370, doi:  
705 10.1016/j.scitotenv.2019.135370, 2019b.
- 706 Ma, R., Yang, G., Duan, H., Jiang, J., Wang, S., Feng, X., Li, A., Kong, F., Xue, B.,  
707 Wu, J., and Li, S.: China’s lakes at present: Number, area and spatial distribution,  
708 *Sci. China Earth. Sci.*, 54, 283–289, doi: 10.1007/s11430-010-4052-6, 2011.
- 709 Ma, Y., Liu, K. -B., Feng, Z., Sang, Y., Wang, W., and Sun, A.: A survey of modern  
710 pollen and vegetation along a south–north transect in Mongolia, *J. Biogeogr.*, 35,  
711 1512–1532, doi: 10.1111/j.1365-2699.2007.01871.x, 2008.
- 712 Meyers, P. A.: Applications of organic geochemistry to paleolimnological  
713 reconstructions: a summary of examples from the Laurentian Great Lakes, *Org.*  
714 *Geochem.*, 34, 261–289, doi: 10.1016/S0146-6380(02)00168-7, 2003.
- 715 Meyers, P. A., and Ishiwatari, R.: Lacustrine organic geochemistry – an overview of



716 indicators of organic matter sources and diagenesis in lake sediments. *Org.*  
717 *Geochem.* 20, 867–900, doi: 10.1016/0146-6380(93)90100-P, 1993.

718 Mykleby, P. M., Snyder, P. K., and Twine, T. E.: Quantifying the trade-off between  
719 carbon sequestration and albedo in midlatitude and high-latitude North American  
720 forests, *Geophys. Res. Lett.*, 44, 2493–2501, doi: 10.1002/2016gl071459, 2017.

721 Prentice, I. C.: Multidimensional scaling as a research tool in Quaternary palynology:  
722 a review of theory and methods, *Rev. Palaeobot. Palynol.*, 31, 71–104, doi:  
723 10.1016/0034-6667(80)90023-8, 1980.

724 Qiang, M., Liu, Y., Jin, Y., Song, L., Huang, X., and Chen, F.: Holocene record of  
725 eolian activity from Genggahai Lake, north-east Qinghai-Tibetan plateau, China,  
726 *Geophys. Res. Lett.* 41, 589–595, doi: 10.1002/2013GL058806, 2014.

727 Qiang, M., Song, L., Chen, F., Li, M., Liu, X., and Wang, Q.: A 16-ka lake-level  
728 record inferred from macrofossils in a sediment core from Genggahai Lake, north-  
729 east Qinghai-Tibetan Plateau (China), *J. Paleolimnol.*, 49, 575–590, doi:  
730 10.1007/s10933-012-9660-z, 2013.

731 Qin, F.: Modern pollen assemblages of the surface lake sediments from the steppe and  
732 desert zones of the Tibetan Plateau. *Sci. China Earth. Sci.*, 64, 425–439, doi:  
733 10.1007/s11430-020-9693-y, 2021.

734 R Core Team, 2021. R, A language and environment for statistical computing, R  
735 Foundation for Statistical Computing, Vienna.

736 Reimer, P. J., Austin, W. E. N., Bard, E., Bayliss, A., Blackwell, P. G., Bronk Ramsey,  
737 C., Butzin, M., Cheng, H., Edwards, R. L., Friedrich, M., Grootes, P. M.,  
738 Guilderson, T. P., Hajdas, I., Heaton, T. J., Hogg, A. G., Hughen, K. A., Kromer, B.,  
739 Manning, S. W., Muscheler, R., Palmer, J. G., Pearson, C., Van Der Plicht, J.,  
740 Reimer, R. W., Richards, D. A., Scott, E. M., Southon, J. R., Turney, C. S. M.,  
741 Wacker, L., Adolphi, F., Büntgen, U., Capano, M., Fahrni, S. M., Fogtmann-Schulz,  
742 A., Friedrich, R., Köhler, P., Kudsk, S., Miyake, F., Olsen, J., Reinig, F., Sakamoto,  
743 M., Sookdeo, A., and Talamo, S.: The IntCal20 Northern Hemisphere Radiocarbon  
744 Age Calibration Curve (0–55 cal kBP), *Radiocarbon*, 62, 725–757,



- 745 <https://doi.org/10.1017/RDC.2020.41>, 2020.
- 746 Schlütz, F., and Lehmkuhl, F.: Holocene climatic change and the nomadic  
747 Anthropocene in Eastern Tibet: palynological and geomorphological results from  
748 the Nianbaoyeze Mountains, *Quat. Sci. Rev.*, 28, 1449–1471, doi:  
749 10.1016/j.quascirev.2009.01.009, 2009.
- 750 Shen, C., Liu, K., Tang, L., and Overpeck, J.: Modern pollen rain in the Tibetan  
751 Plateau, *Front. Earth Sci.* 9, 732441, doi: 10.3389/feart.2021.732441, 2021.
- 752 Shen, J., Liu, X. Q., Wang, S. M., and Matsumoto, R.: Palaeoclimatic changes in the  
753 Qinghai Lake area during the last 18,000 years, *Quat. Int.*, 136,131-140, doi:  
754 10.1016/j.quaint.2004.11.014, 2005.
- 755 Sun, X., Zhao, Y., and Li, Q.: Holocene peatland development and vegetation changes  
756 in the Zoige Basin, eastern Tibetan Plateau, *Sci. China Earth. Sci.*, 47, 1097–1109,  
757 doi: 10.1007/s11430-017-9086-5, 2017.
- 758 Tang, L., Mao, L., Shu, J., Li, C., Shen, C., and Zhou, Z.: An Illustrated Handbook of  
759 Quaternary Pollen and Spores in China. Science Press, Beijing, 2017. (In Chinese  
760 with English summary)
- 761 ter Braak, C. J. F. and Verdonschot, P. F. M.: Canonical correspondence analysis and  
762 related multivariate methods in aquatic ecology, *Aquat. Sci.*, 57, 255–289, doi:  
763 10.1007/BF00877430, 1995.
- 764 ter Braak, C. J. F. and Prentice, I. C.: A theory of gradient analysis, *Adv. Ecol. Res.*,  
765 18, 271–317, doi: 10.1016/S0065-2504(08)60183-X, 1988.
- 766 Wang, F. X., Qian, N. F., Zhang, Y. L., and Yang, H. Q.: Pollen Flora of China.  
767 Science Press, Beijing, 1995. (In Chinese)
- 768 Wang, H., Hu, Y., Zhang, X., Lv, F., Ma, X., W, D., Chen, F., Zhou, A., Hou, J., and  
769 Chen, J.: A 17 ka multi-proxy paleoclimatic record on the north-east Tibetan  
770 Plateau: implications for the northernmost boundary of the Asian summer monsoon  
771 during the Holocene. *Int. J. Climatol.*, 42, 191–201, doi: 10.1002/joc.7239, 2021.
- 772 Wang, X., Yi, S., Lu, H., Vandenberghe, J., and Han, Z.: Aeolian process and climatic  
773 changes in loess recorded from the NTP: response to global temperature forcing



- 774 since 30 ka. *Paleoceanogr. Paleoclim.* 30, 612–620, doi: 10.1002/2014PA002731,  
775 2015.
- 776 Wang, Y., Herzschuh, U., Shumilovskikh, L., Mischke, S., Birks, H. J. B.,  
777 Wischnewski, J., Böhner, J., Schlütz, F., Lehmkuhl, F., Diekmann, B., Wünnemann,  
778 B., and Zhang, C.: Quantitative reconstruction of precipitation changes on the NE  
779 Tibetan Plateau since the Last Glacial Maximum – extending the concept of pollen  
780 source area to pollen-based climate reconstructions from large lakes, *Clim. Past.*,  
781 10, 21–39, doi: 10.5194/cp-10-21-2014, 2014.
- 782 Wang, Y., Cheng, H., Edwards, R. L., An, Z., Wu, J., Shen, C., and Dorale, J. A.: A  
783 high-resolution absolute-dated Late Pleistocene monsoon record from Hulu Cave,  
784 China, *Science*, 294, 2345–2348, doi: 10.1126/science.1064618, 2001.
- 785 Wei, H., Ma, C., Zhang, J., Sun, Y., Li, Q., Hou, G., and Duan, R.: Climate change  
786 and anthropogenic activities in Qinghai Lake basin over the last 8500 years derived  
787 from pollen and charcoal records in an aeolian section, *Catena*, 193, 104616, doi:  
788 10.1016/j.catena.2020.104616, 2020.
- 789 Wischnewski, J., Mischke, S., Wang, Y., and Herzschuh, U.: Reconstructing climate  
790 variability on the north-east Tibetan Plateau since the last Lateglacial—a multi proxy,  
791 dual-site approach comparing terrestrial and aquatic signals, *Quat. Sci. Rev.*, 30,  
792 82–97, doi: 10.1016/j.quascirev.2010.10.001, 2011.
- 793 Xiao, J., Fan, J., Zhou, L., Zhai, D., Wen, R., and Qin, X.: A model for linking grain-  
794 size component to lake level status of a modern clastic lake. *J. Asian. Earth. Sci.*  
795 69, 149–158, doi: 10.1016/j.jseaes.2012.07.003, 2013.
- 796 Xu, D., Lu, H., Wu, N., Liu, Z., Li, T., Shen, C., and Wang, L.: Asynchronous marine-  
797 terrestrial signals of the last deglacial warming in East Asia associated with low-  
798 and high-latitude climate changes, *Proc. Natl. Acad. Sci. USA.*, 110, 9657–9662,  
799 doi: 10.1073/pnas.1300025110, 2013.
- 800 Xu, Q., Li, Y., Yang, X., and Zheng, Z.: Quantitative relationship between pollen and  
801 vegetation in northern China, *Sci. China Ser. D-Earth. Sci.*, 50, 582–599, doi:  
802 10.1007/s11430-007-2044-y, 2007.



- 803 Yan, D., and Wünnemann, B.: Late Quaternary water depth changes in Hala Lake,  
804 northeastern Tibetan Plateau, derived from ostracod assemblages and sediment  
805 properties in multiple sediment records, *Quat. Sci. Rev.*, 95, 95–114, doi:  
806 10.1016/j.quascirev.2014.04.030, 2014.
- 807 Yang B, Tang L., Brauning, A., Davis, M. E., Shao, J., and Liu, J.: Summer  
808 temperature reconstruction on the central Tibetan Plateau during 1860–2002 derived  
809 from ice core pollen, *J. Geophys. Res - atmos.*, 113, doi: 10.1029/2008JD010142,  
810 2008.
- 811 Yao, Z.: Ice-core pollen studies from the Dunde and Guliya Ice Caps, Qinghai-Tibetan  
812 Plateau, China, PhD Dissertation, Baton Rouge: Louisiana State University, USA,  
813 2000.
- 814 Yu, G., Tang, L., Yang, X., Ke, X., and Harrison, S. P.: Modern Pollen Samples from  
815 Alpine Vegetation on the Tibetan Plateau. *Global Ecol. Biogeogr.* 10, 503–519, doi:  
816 10.1046/j.1466-822x.2001.00258.x, 2001.
- 817 Zhao, Y., and Herzsuh, U.: Modern pollen representation of source vegetation in the  
818 Qaidam Basin and surrounding mountains, north-eastern Tibetan Plateau, *Veget.*  
819 *Hist. Archaeobot.*, 18, 245–260, doi: 10.1007/s00334-008-0201-7, 2009.
- 820 Zhao, Y., Liu, Y., Guo, Z., Fang, K., Li, Q., Cao, X.: Abrupt vegetation shifts caused  
821 by gradual climate changes in central Asia during the Holocene. *Sci. China Earth*  
822 *Sci.*, 60, 1317–1327, doi: 10.1007/s11430-017-9047-7, 2017.
- 823 Zhao, Y., Tzedakis, P. C., Li, Q., Qin, F., Cui, Q., Liang, C., Birks, H. J. B., Liu, Y.,  
824 Zhang, Z., Ge, J., Zhao, H., Felde, V. A., Deng, C., Cai, M., Li, H., Ren, W., Wei,  
825 H., Yang, H., Zhang, J., Yu, Z., and Guo, Z.: Evolution of vegetation and climate  
826 variability on the Tibetan Plateau over the past 1.74 million years, *Sci. Adv.*, 6,  
827 eaay6193, doi: 10.1126/sciadv.aay6193, 2020.
- 828 Zhao, Y., Yu, Z., and Zhao, W.: Holocene vegetation and climate histories in the  
829 eastern Tibetan Plateau: controls by insolation-driven temperature or monsoon-  
830 derived precipitation changes? *Quat. Sci. Rev.*, 30, 1173–1184, doi:  
831 10.1016/j.quascirev.2011.02.006, 2011.



832 Zhao, Y., Yu, Z., Chen, F., Ito, E., and Zhao, C.: Holocene vegetation and climate  
833 history at Hurlig Lake in the Qaidam Basin, northwest China, *Rev. Palaeobot.*  
834 *Palynol.*, 145, 275–288, doi: 10.1016/j.revpalbo.2006.12.002, 2007.

835 Zhou, W., Yu, S., Burr, G. S., Kukla, G. J., Jull, A. J. T., Xian, F., Xiao, J., Colman, S.  
836 M., Yu, H., Liu, H., Liu, Z., and Kong, X.: Postglacial changes in the Asian summer  
837 monsoon system: A pollen record from the eastern margin of the Tibetan Plateau.  
838 *Boreas*, 39: 528–539, doi: 10.1111/j.1502-3885.2010.00150.x, 2010.

839 Zhu, L., Lü, X., Wang, J., Peng, P., Kasper, T., Daut, G., Haberzettl, T., Frenzel, P., Li,  
840 Q., Yang, R., Schwalb, A., and Mäusbacher, R.: Climate change on the Tibetan  
841 Plateau in response to shifting atmospheric circulation since the LGM, *Sci. Rep.*, 5,  
842 13318, doi: 10.1038/srep13318, 2015.

843

844

845

846

847

848

849

850

851

852

853

854

855

856

857

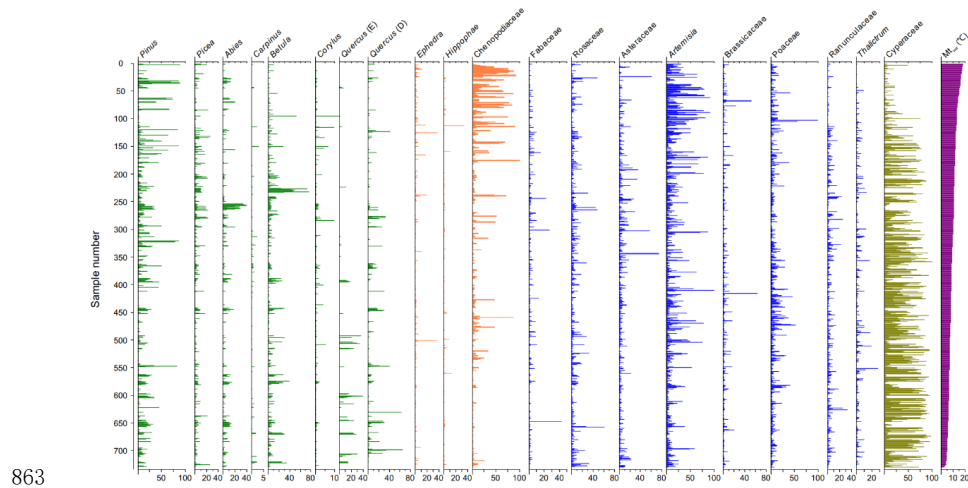
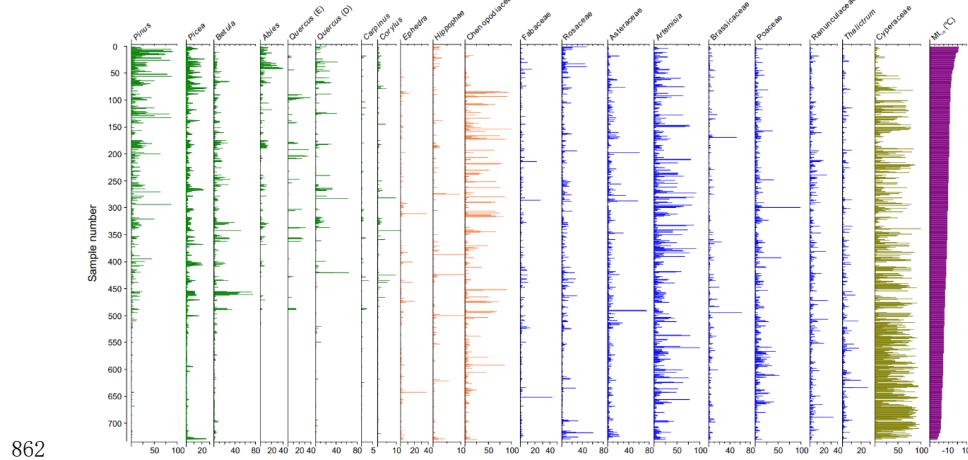
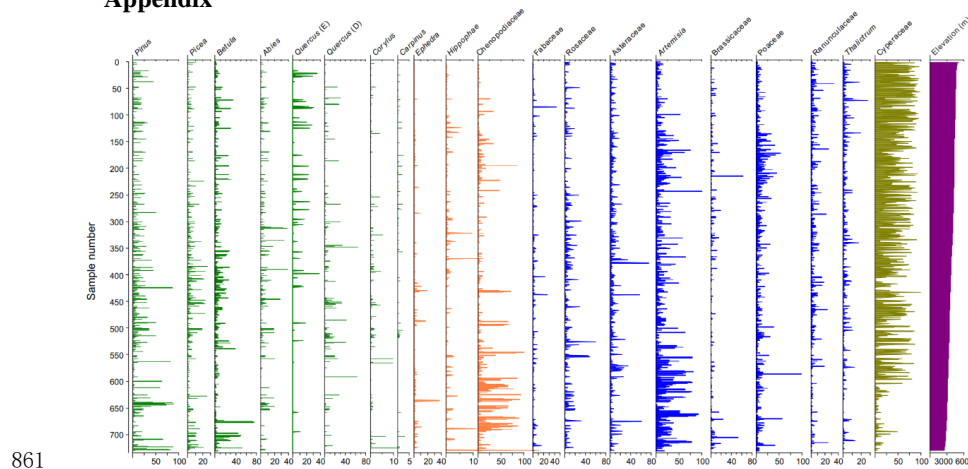
858

859

860



### Appendix



864 **Figure A1.** Pollen assemblage of the surface sediment samples with climate data (Elev,  $Mt_{co}$ , and



865  $M_{t_{wa}}$  from eastern Tibetan Plateau. Elev: Elevation (m);  $M_{t_{co}}$ : mean temperature of the coldest

866 month ( $^{\circ}\text{C}$ );  $M_{t_{wa}}$ : mean temperature of the warmest month ( $^{\circ}\text{C}$ ).